PAPER

High capacity lithium ion batteries composed of cobalt oxide nanoparticle anodes and Raman spectroscopic analysis of nanoparticle strain dynamics in batteries

IOP Publishing Nanotechnology
Nanotechnology 29 (2018) 075403 (10pp) https://doi.org/10.1088/1361-6528/aaa231

High capacity lithium ion batteries composed of cobalt oxide nanoparticle anodes and Raman spectroscopic analysis of nanoparticle strain dynamics in batteries

Mohammad A Islam[1], Mateusz Zuba[1], Vincent DeBiase[1], Nicholas Noviasky[1] and Christopher J Hawley[2]

[1] Department of Physics, State University of New York at Oswego, Oswego, NY 13126, United States of America
[2] Department of Materials Science and Engineering, Drexel University, Philadelphia, PA 19104, United States of America

E-mail: mohammad.islam@oswego.edu

Received 17 October 2017, revised 13 December 2017
Accepted for publication 15 December 2017
Published 15 January 2018

Abstract

Cobalt nanoparticle thin films were electrophoretically deposited on copper current collectors and were annealed into thin films of hollow Co_3O_4 nanoparticles. These thin films were directly used as the anodes of lithium ion batteries (LIBs) without the addition of conducting carbons and bonding agents. LIBs thus fabricated show high gravimetric capacities and long cycle lives. For $\approx$1.0 μm thick Co_3O_4 nanoparticle films the gravimetric capacities of the batteries were more than 800 mAh g^{-1} at a current rate of C/15, which is about 90% of the theoretical maximum. Additionally, the batteries were able to undergo 200 charge/discharge cycles at a relatively fast rate of C/5 and maintain 50% of the initial capacity. In order to understand the electrochemistry of lithiation in the context of nanoparticles, Raman spectra were collected at different stages of the electrode cycles to determine the chemical and structural changes in the nanomaterials. Our results indicate that initially the electrode nanoparticles were under significant strain and as the battery underwent many cycles of charging/discharging the nanoparticles experienced progressive strain relaxation.

Supplementary material for this article is available online

Keywords: nanoparticles, lithium ion battery, Raman spectroscopy, electrophoretic deposition

(Some figures may appear in colour only in the online journal)

Introduction

The high negative potential of lithium (and other alkali metals) that makes it attractive as a cathode material in rechargeable batteries, however results in a violent reaction of the metal with aqueous electrolytes. Consequently, practical lithium batteries were possible only with the introduction of aprotic electrolytes [1]. Because of their high specific energies in terms of area, volume, and mass rechargeable lithium ion batteries (LIBs) have become the power source of choice for handheld devices, electronics, electric vehicles and even airliners. In spite of the obvious advantages, however, the overall share of LIBs in the rechargeable battery market is small due to several factors including high cost related to the need for carefully purified materials, electrode degradation, relatively slow charging rates, and safety issues [2].

It has already been proven decisively that nanostructuring of electrodes contributes to significant improvement in the overall performance of LIBs [3–6]. The unique advantages nanostructuring provides to LIB technology include short

diffusion times that improve battery speed, higher surface to volume ratio rendering more reactive sites available for electrochemical reactions and thus increasing battery capacity, and the intrinsic expandability of nanosystems contributing to amenability to large and repeated volume changes demanded by repeated conversion reactions and lithiation. Less prominent yet important advantages of nanomaterials in LIBs are cost effective solution synthesis and processability, and versatility in the different kind of nanomaterials that can be used in LIB fabrication [7–9].

Application of nanomaterials in the forms of nanorods and nanosheets and more recently in the form of nanoparticles have resulted in impressive battery performance. Recent applications include nanoparticles of Fe_3O_4, Fe_2O_3, MnO, and Co_3O_4, nanosheets of MXenes and MoS_2, silicon nanowires, and graphene wrapped sulfur particles [2, 5–7, 10–15]. Co_3O_4, due to its interesting chemical, catalytic, and photovoltaic properties, has been the subject of wide range of experimental and theoretical investigations. Application of Co_3O_4 in LIBs in forms of nanoparticles, nanowires, nanocages, nanotubes and in composite forms with graphene have resulted in impressive capacity retention and cyclability [5, 6, 16–19].

Many reports on the application of nanomaterials in LIBs, however, have focused on the end result which is the improvement of battery speed and capacity. Very often several active materials are mixed in systematic proportions along with conductive carbons to improve charge conductivity and polymeric binders to improve mechanical stability of the electrodes, and battery functionalities are studied as a function of these mixtures. While these ad hoc methods have resulted in impressive battery performance, it is difficult to generalize these methods for the practical applications of LIBs. Some experiments which measured LIB performance did not systematically distinguish the different material processes associated with the fabrication. It is indeed difficult to extract the unique nanoscale physics of the active materials from the result of these batteries that are composed of several components.

Perhaps as important as the construction of the battery, is the analyses of battery performance, which have very often focused on the physical aspects of the nanomaterials. Several groups have investigated the electrochemistry of LIBs as a function of nanoparticle size, shape and surface coverage using x-ray diffraction (XRD), scanning electron microscopy (SEM), and transmission electron microscopy (TEM) [5, 12, 13]. TEM studies, for example, showed that repeated intercalation of Li ion into the nanoparticle matrix and the conversion reactions result in pulverization of larger nanoparticles into more stable smaller size nanoparticles [5].

Nanoparticles, however, possess unique characteristics besides sizes, shapes and ligand coverage. It has been shown, at least for oxide nanoparticles, that the lattice constant increases as the particle diameter decreases, resulting in surface strain [20, 21]. Surface impurities and surface strains are important parameters for nanoparticles that can directly influence the electrochemistry of lithiation in LIBs. These nanoscale unique properties have received disproportionately less attention in LIB research.

In this work cobalt (Co) nanoparticle thin films were electrophoretically deposited on copper current collectors and were annealed into thin films of hollow Co_3O_4 nanoparticles, which were directly used as the anodes in fabricating half-cell LIBs (H-LIBs). The application of electrophoretic deposition (EPD) resulted in electrodes composed of only Co_3O_4 nanoparticles without the need for any polymeric binders and conducting carbons. The EPD films are found to be mechanically much stronger when compared to the conventional slurry cast films and the thickness of the EPD films are tunable within a fraction of a micron. H-LIBs fabricated thus show high gravimetric capacities and long cycle lives. For $\approx$1.0 μm thick Co_3O_4 nanoparticle films the gravimetric capacities of the H-LIBs were more than 800 mAh g^{-1} at a current rate of $C/15$ which is about 90% of the theoretical maximum. Additionally, the H-LIBs were able to undergo 200 charge/discharge cycles at relatively fast rate of $C/5$ and maintain 50% of the initial capacity. In order to understand the electrochemistry of lithiation in the context of nanoparticles, we used Raman spectroscopy at different stages of the battery cycles to determine the chemical and structural changes in the nanoparticle films. Our results indicate that the pristine Co_3O_4 nanoparticles in the freshly prepared anode are under significant strain and as the battery undergoes cycles the nanoparticles experience progressive strain relaxation. These results corroborate the TEM images in [5] where it is shown that upon many cycles of charging/discharging the anode material takes on the morphology of a disordered material. Additionally, we find that upon discharging an incomplete conversion of the Co_3O_4 nanoparticles into Li_2O and elemental Co takes place. However, upon charging we find scant Raman signature of Li_2O and elemental Co on the anode indicating complete conversion of the discharge products back to Co_3O_4.

Experimental methods

Materials synthesis

Cobalt nanoparticles were synthesized by following the literature recipe of Puntes *et al* [22]. All chemical reagents were purchased from Sigma Aldrich. 0.52 g $Co_2(CO)_8$ was dissolved in 4 ml of dichlorobenzene and the solution was stirred at room temperature for about an hour until the cobalt solution dissolved completely. In a triple-necked flask, 0.1 g TOPO and 0.09 g of oleic acid were added to 12 ml of dichlorobenzene. The solution was vacuumed for about half an hour, then the temperature was set to 180 °C and the solution was placed under N_2 flushing. When the temperature stabilized to 180 °C the $Co_2(CO)_8$ solution was added quickly. The solution was left at 180 °C for about 5 min, then the reaction was stopped and the final product was cooled using a room temperature water bath. The Co nanoparticles were cleaned off the original solution and unreacted reagents using the size

selective precipitation method by first using ethanol and then acetone as the non-solvents, and hexane as the solvent.

Electrophoretic deposition

As shown in figure S1, available online at stacks.iop.org/NANO/29/075403/mmedia, a pair of copper electrodes, cut in circular shapes of ~1 cm in diameter, are placed 1.8 mm apart in a parallel plate capacitor configuration and secured on a stable platform. A solution of Co nanoparticles in hexane is prepared by sonication. The electrode assembly is then slowly submerged in the solution and DC voltages in the range of 300–600 V are applied between the electrodes. After a few minutes, thin films of Co nanoparticles are seen to develop on both plates when the voltage is turned off and the electrodes are removed from the solution. The EPD films are subsequently annealed in an oven in the ambient at 200 °C for 6 h to convert the Co nanoparticles into hollow Co_3O_4 nanoparticles [23].

Materials characterization

The Co nanoparticles and the EPD Co_3O_4 nanoparticle films were characterized using a FEI F20 TEM, a JEOL JSM-6610LV SEM, a Nanomagnetic Instruments atomic force microscope (AFM) in the tapping mode, and optical microscopes. The crystallinity of the nanoparticles was determined using a Bruker Instruments x-ray diffractometer. The film thicknesses were measured by AFM, as described in the supplementary information.

Battery fabrication

H-LIBs were fabricated using the EPD Co_3O_4 nanoparticle films as the working electrode in both Swagelok-type and 2032 size coin-type electrochemical cells. A lithium foil was used as the counter electrode, 1 M $LiPF_6$ in a 50:50 w/w mixture of ethylene carbonate and diethyl carbonate was used as the aprotic electrolyte and a Celgard 2400 polypropylene separator completed the device.

Raman spectroscopy

Raman scattering spectra were collected at 293 K in air from the Co_3O_4 nanoparticle anodes at different stages of the battery cycles. For Raman spectroscopy only Swagelok cells were used since it is easier to disassemble these batteries. Four Swagelok cells were assembled using EPD Co_3O_4 nanoparticle film anodes with almost identical film thicknesses of ≈1.2 μm. The first battery was stopped after the first discharge, the second was stopped after the first discharge/charge cycle, the third was stopped after the 25th discharge/charge cycle and the fourth was stopped after the 100th discharge/charge cycle. The batteries were disassembled and the Co_3O_4 nanoparticle anodes retrieved. The anodes were gently cleaned with ethanol to remove trace electrolytes. Raman spectra were collected from each of these electrodes as well as a pristine EPD Co_3O_4 nanoparticle anode. Raman scattering spectra were excited using the linearly polarized output of a solid state laser (532 nm) with 13.6 mW of power in a spot diameter of ≈1.0 μm at the sample, and were dispersed and detected using a single-axis monochromator equipped with a charge-coupled detector array (Horiba XploRA, Edison NJ). All Raman spectra were collected unpolarized and in the backscattering geometry.

Results and discussions

EPD of Co nanoparticles

Scalable nanomanufacturing requires nanomaterial assembly methods that are repeatable, durable, environmentally safe, and result in films that are mechanically robust, possess interparticle connectivity and patternable. This places severe demands on the methodologies to be used in forming nanomaterial assemblies. Conventional methods of slurry cast and spin cast that are used in bulk materials are hardly applicable for assembling nanoparticles. Accordingly, nanoparticle films formed by such methods are fragile and lack interdot connectivity. Recently advances have been made through ligand exchange mechanisms whereby the original and sometimes bulky ligands are replaced by shorter and conducting linkers to improve interdot connectivity [24, 25]. However, this could potentially add a new component to consider while extracting the unique nanoscale physics in modeling the results.

A strong alternative in the form of EPD has emerged over the last few years and has already progressed significantly in addressing the problems associated with large-scale and well-controlled assembly of nanoparticles [26–28]. Recent applications of EPD in nanomanufacturing include orders of magnitude enhancement in the conductivity of nanoparticle thin films, fabrication of nanocomposites for improving antibiotic delivery and graphene nanocomposites for application in solar cells and field effect transistors [29–32].

Using a setup as shown in figure S1, we deposited Co nanoparticles onto copper substrates that were subsequently converted into films of hollow Co_3O_4 nanoparticles, and were directly used as the anodes in H-LIBs. The film thickness was found to be dependent on the deposition time, nanoparticle density in the solution, and the voltage applied. For a typical electrode separation of 1.8 mm, 550 V DC and 10 min of deposition, the film thicknesses were found to be between 1 and 3 μm.

The results between the conventional slurry cast or spin coated films and the EPD films are stark. Whereas the conventional methods result in significant amount of material waste, EPD has almost zero waste and the film thickness can be controlled within a fraction of a micron, as shown in figure S3. Once a film is deposited the remaining nanoparticle solution can be used for the next film or can be saved for later use. EPD results in Co_3O_4 nanoparticle films on copper current collectors without the need for any polymeric binders and conducting carbons. Standard DC conductivity measurements carried out on EPD Co_3O_4 nanoparticle films and on dry cast films show that the former is at least an order of magnitude more conducting, as shown in figure S4. Further extensive comparative studies between the conventional slurry cast

films and the EPD films have been reported demonstrating the superior mechanical stability of the latter films in [5], where one of us was a co-author. This paper will only focus of H-LIBs fabricated with EPD films.

Properties of the Co nanoparticles and the electrophoretically deposited Co_3O_4 nanoparticle anodes

The Co nanoparticles and the EPD Co_3O_4 nanoparticle anodes were analyzed using visible microscopy, TEM, SEM, AFM, and XRD. The as synthesized Co nanoparticles were approximately 11.87 ± 1.16 nm in diameter as shown in the TEM images of figures 1(a) and (b), and as described in the supplementary information. HRTEM image (figure 1(b)) shows lattice fringes that demonstrates that the nanoparticles are crystalline.

The TEM image in figure 1(c) shows that the Co nanoparticles have converted into hollow Co_3O_4 nanoparticles upon annealing. The well-known Kirkendall effect that is responsible for such hollow oxide nanoparticle formation results in two reactive surfaces—the outer surface and the inner surface—on each nanoparticle that could make these nanoparticle film anodes useful for faster LIBs [22, 23].

Figures 1(d)–(f) are micrographs of the EPD films. The optical micrograph in figure 1(d) shows that the Co_3O_4 nanoparticle films are cm in lateral dimensions and that the films crack as the residual solvents evaporate once EPD is completed. The AFM image of figure 1(e) shows that the cracks are about 1 μm in width and are quite pervasive and the higher magnification SEM image of figure 1(f) shows dense packing of the Co_3O_4 nanoparticle in the EPD films.

XRD patterns shown in figure 1(g) show that the as synthesized Co nanoparticles crystallize in ε-Co phase as seen previously [22, 23]. The Co nanoparticles got converted to Co_3O_4 nanoparticles upon 6 h of annealing at 200 °C, as shown in the XRD pattern in figure 1(g). Since XRD was performed on the EPD Co_3O_4 nanoparticle films on copper substrates, we see the x-ray peaks of the substrate as well in the two annealed films.

Electrochemical performance of the electrophoretically deposited Co_3O_4 anodes in H-LIBs

The electrochemical reactions in LIBs with Co_3O_4 anodes have been shown to be [5, 6]:

$$Co_3O_4 + 8e^- + 8Li^+ \leftrightarrow 4Li_2O + 3Co. \quad (1)$$

Several studies have indicated that following the first discharge the following reaction takes place with the formation of CoO:

$$Co + Li_2O \leftrightarrow CoO + 2e^- + 2Li^+. \quad (2)$$

The electrochemical properties of the H-LIBs formed with EPD Co_3O_4 nanoparticle film anodes were tested using cyclic voltammetry (CV) and galvanostatic charge/discharge cycles at different rates and as a function of film thickness. CV measurements that shed insights into the redox reactions of the battery were performed at a rate of 0.1 mV s^{-1} in the range of 0.2–3.0 V. As shown in figure 2(a) the first cycle shows a major broad oxidation peak at 2.1 V and one major reduction peak at 0.56 V. On subsequent cycles the major oxidation peak shifts to 2.16 V whereas the main reduction peak shifts to 0.95 V at the end of the sixth cycle. These trends are similar to what have been seen in other Co_3O_4 nanomaterials based LIBs [5]. The smaller satellite peaks around the major peaks are due to fact that Co_3O_4, as discussed in Raman analysis section later, is composed of Co^{3+} and Co^{2+} ions, and the oxidation and the reduction voltages of these species are different. Detailed CV analysis of Co_3O_4 nanomaterial based batteries is available in literature [5, 8].

Figures 2(b) and (c) show the galvanostatic charge/discharge at rates C/15, C/7.5, C/5, C/3 and finally back to C/15, each for five cycles for an H-LIB fabricated with 1.2 μm thick Co_3O_4 nanoparticle film. The first discharge capacity is found to be more than 1800 mAh g^{-1} which is more than the theoretical value of 890 mAh g^{-1} that can be determined from equation (1). Significantly larger discharge time and discharge capacity for the first cycle have routinely been seen other published reports [5].

The 'extra' capacity is probably due to the formation of the solid electrolyte interface (SEI) and parasitic capacitance that are characteristics of thin film electrode batteries. An additional contribution in our H-LIBs could be from copper oxide thin films that might have formed on the copper current collectors when the EPD Co nanoparticles were being oxidized in the oven.

To determine the contribution of copper oxide to the overall capacity, H-LIBs were formed with bare copper plate anodes after being oxidized at the same temperature and duration as those used for converting Co into Co_3O_4. As shown in the inset of figure 2(b), the average capacity of these 'null' batteries was found to be 89 mAh g^{-1} at the first discharge that decreased to 18 mAh g^{-1} at the end of the 10th cycle. From this we determine that the contribution of copper oxide to the overall capacity in our H-LIBs is negligible.

The gravimetric capacity decreases to 802 mAh g^{-1} at the first charge cycle at C/15 which is almost 90% of the theoretical value. The capacity decreases as the current is increased and reaches 303 mAh g^{-1} at the maximum current of 0.5 mA, C/3. The capacity, however, recovers almost to the initial 800 mAh g^{-1} range when the current is cycled back to the C/15 rate. These capacities should be compared with those of the graphite electrodes (372 mAh g^{-1}) that are used in commercial LIBs.

In order to determine the cycle lives of the H-LIBs formed with EPD Co_3O_4 nanoparticle films we subjected the H-LIBs to continuous charging/discharging at a rate of C/5. As shown in figure 2(d), the H-LIBs, starting with an initial capacity of 606 mAh g^{-1}, retained a capacity of 300 mAh g^{-1}

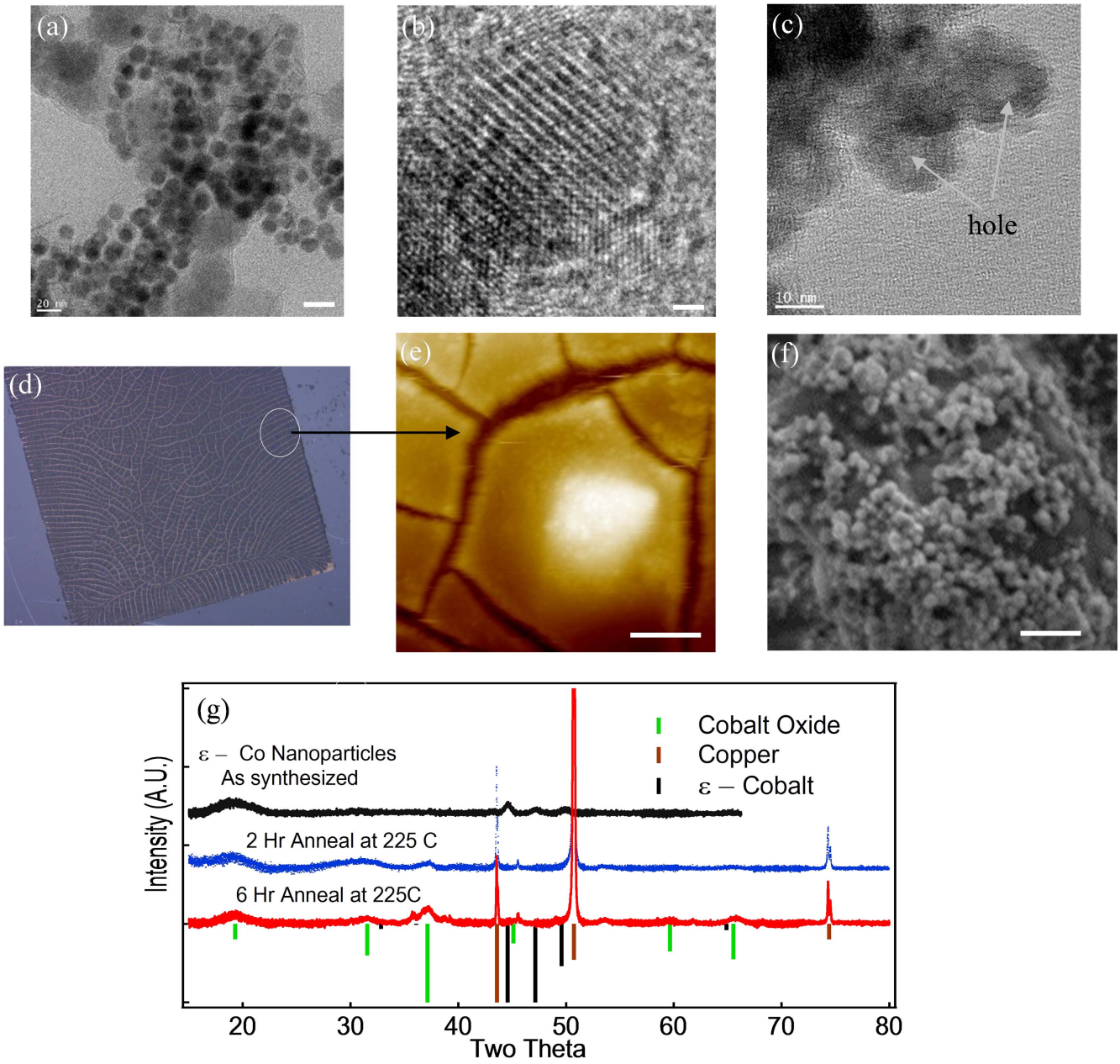

Figure 1. Nanomaterial synthesis and characterization for H-LIB anodes. TEM image of Co nanoparticles (a) upon synthesis and size selective precipitation shows an average diameter of the nanoparticles to be 11.87 ± 1.16 nm. HRTEM (b) shows lattice fringes that demonstrates that the nanoparticles are crystalline. TEM image of Co_3O_4 nanoparticles (c) shows that the solid Co nanoparticles get converted into hollow Co_3O_4 nanoparticles upon annealing in the ambient. The optical micrographs (d) and low magnification AFM image (e) show that the EPD nanoparticle films crack due to post deposition solvent evaporation and that the films are flat. SEM image (f) shows that EPD results in dense packing of the nanoparticles. XRD spectra (g) of cobalt nanoparticle powder and of the Co_3O_4 nanoparticle film on copper current collector and comparison with the reference data for ε-Co and bulk Co_3O_4 show the crystallinity of the nanomaterials. Also seen are the x-ray features from the copper substrate. The scale bars in (a), (b), (c), (e) and (f) are 20 nm, 2 nm, 10 nm, 1 μm and 40 nm, respectively.

at the end of 200 cycles when the capacity dropped precipitously.

In order to determine the capacity dependence on nanoparticle film thickness H-LIBs were also fabricated with Co_3O_4 nanoparticle film anodes of thicknesses 3.4 and 0.8 μm. As shown in figure 2(d) the capacity with the 3.4 μm thick anode was significantly lower than that of the H-LIB with 1.2 μm thick anode and the capacity of the H-LIB with 0.8 μm anode thickness was comparable to that of the H-LIB with 1.2 μm anode thickness. We conclude from these results that H-LIBs formed with EPD Co_3O_4 nanoparticle film anodes will exhibit the best performance with anode thicknesses in the range of 1.0 μm.

We note that the capacity of the H-LIBs that we are fabricating in our lab, while significantly better than the current state of the art graphite electrodes, are, however, less than those reported in previous literature [5, 33]. For example in [5], in which one of us was a co-author, the capacity was

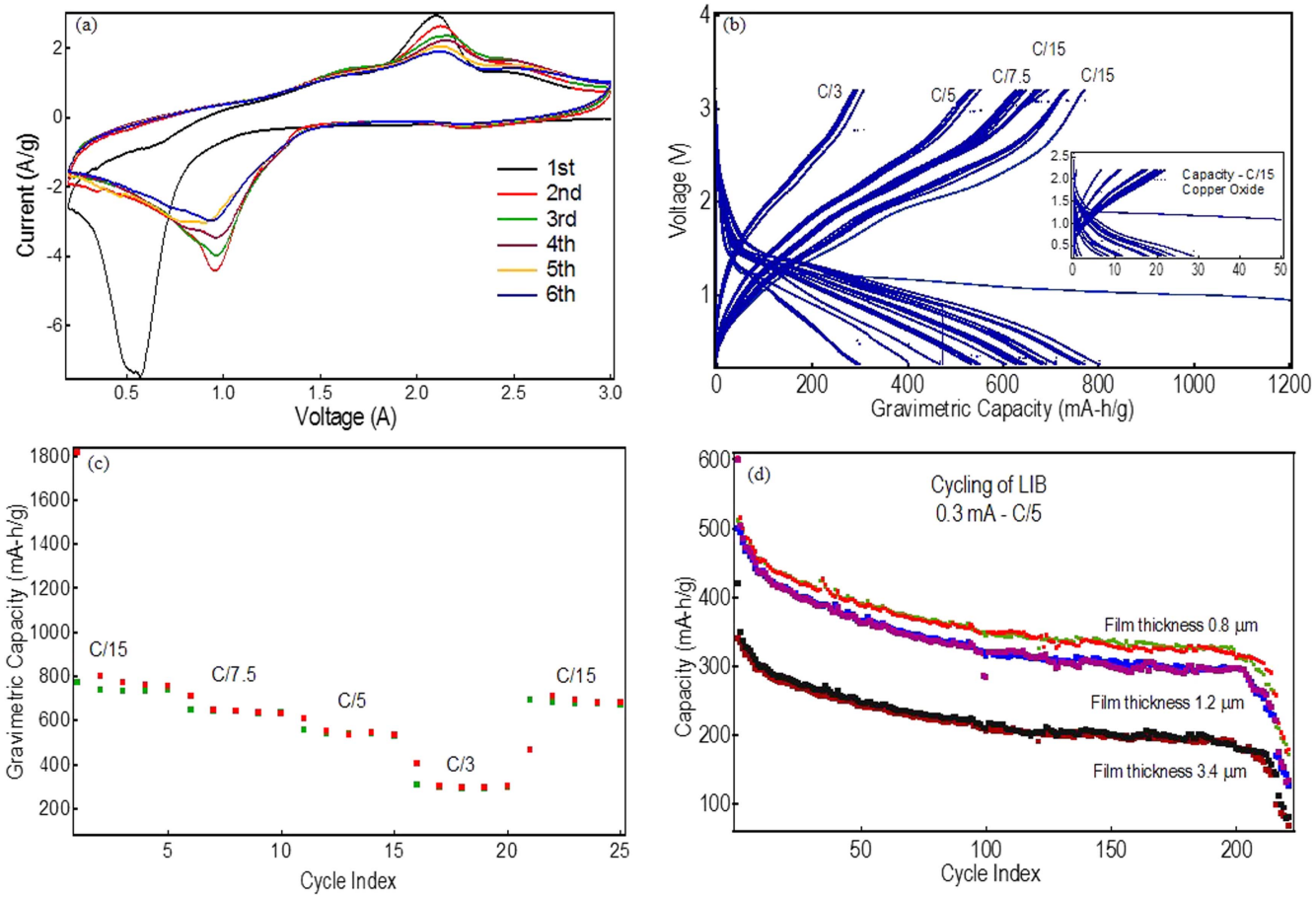

Figure 2. Electrochemical properties of H-LIBs with Co_3O_4 nanoparticle film anodes. First cycle cyclic voltammetry (a) shows major oxidation and reduction peaks at 2.1 V and 0.56 V, respectively. On subsequent cycles the major oxidation peak shifts to 2.16 V whereas the main reduction peak shifts to 0.95 V at the end of the sixth cycle. Galvanostatic charge/discharge at different current rates (b) and (c) show gravimetric capacity retention and recovery after 25 cycles. The inset shows that the contribution from copper oxide to the overall capacity is negligible. Cycle lives of H-LIBs fabricated with Co_3O_4 nanoparticle film anode of different thicknesses show (d) that H-LIBs fabricated using our methods retain at least 50% of the original capacity after almost 200 cycles and that the optimum performance is seen in H-LIBs with anode thickness of approximately 1 μm.

reported to be near the theoretical maximum value of 890 mAh g^{-1} at the end of 50 cycles of charge/discharge at C/20 rate. This requires almost 100% of the Co_3O_4 nanoparticles getting converted into LiO_2 and elemental Co on discharge, and 100% of the LiO_2 and Co reconstituting into Co_3O_4 nanoparticles upon charge. This is indeed an extremely stringent requirement. Formation of nanoparticles requires the constituent reagents to be mixed at the right temperature, formation of nuclei and Oswald ripening. How these exact parameters are achieved inside a LIB is not clear to us. We demonstrate later through Raman spectroscopy that a portion of the nanoparticles in our H-LIBs do not participate in the chemical reaction and that the nanoparticles undergo significant strain release as the battery progresses through its cycles.

Raman spectroscopic analysis of Co_3O_4 nanoparticle anodes in H-LIBs

Raman spectroscopy has been found to be advantageous for materials characterization over other diagnostic tools like TEM, XRD, XPS and photoluminescence due to the facts that the former method is noninvasive and nondestructive, requires little or no sample preparation steps, can be performed either in the ambient or at the same conditions at which a material is to be used in a typical application, and finally, it does not require the material to possess a specific bandgap. Accordingly, Raman scattering has been widely used in identifying structural and electronic phases in solids, thin films, and nanostructured semiconductor and oxide materials, since scattering by phonons and electronic degrees of freedom together provide unique signatures of atomic, polar and electronic ordering [34–38].

Despite its wide range of potential reports on Raman spectroscopic studies in battery technology is few and far between. The electrochemistry of LIBs composed of Co_3O_4 thin film anodes was investigated using XRD and Raman spectroscopy by Liu *et al* [8]. Raman and infrared spectroscopy has been used lately to investigate the formation of SEI in Li and Na based batteries [39, 40]. To the best of our knowledge no Raman studies have been undertaken to investigate the electrochemistry of LIBs composed of Co_3O_4 nanoparticles.

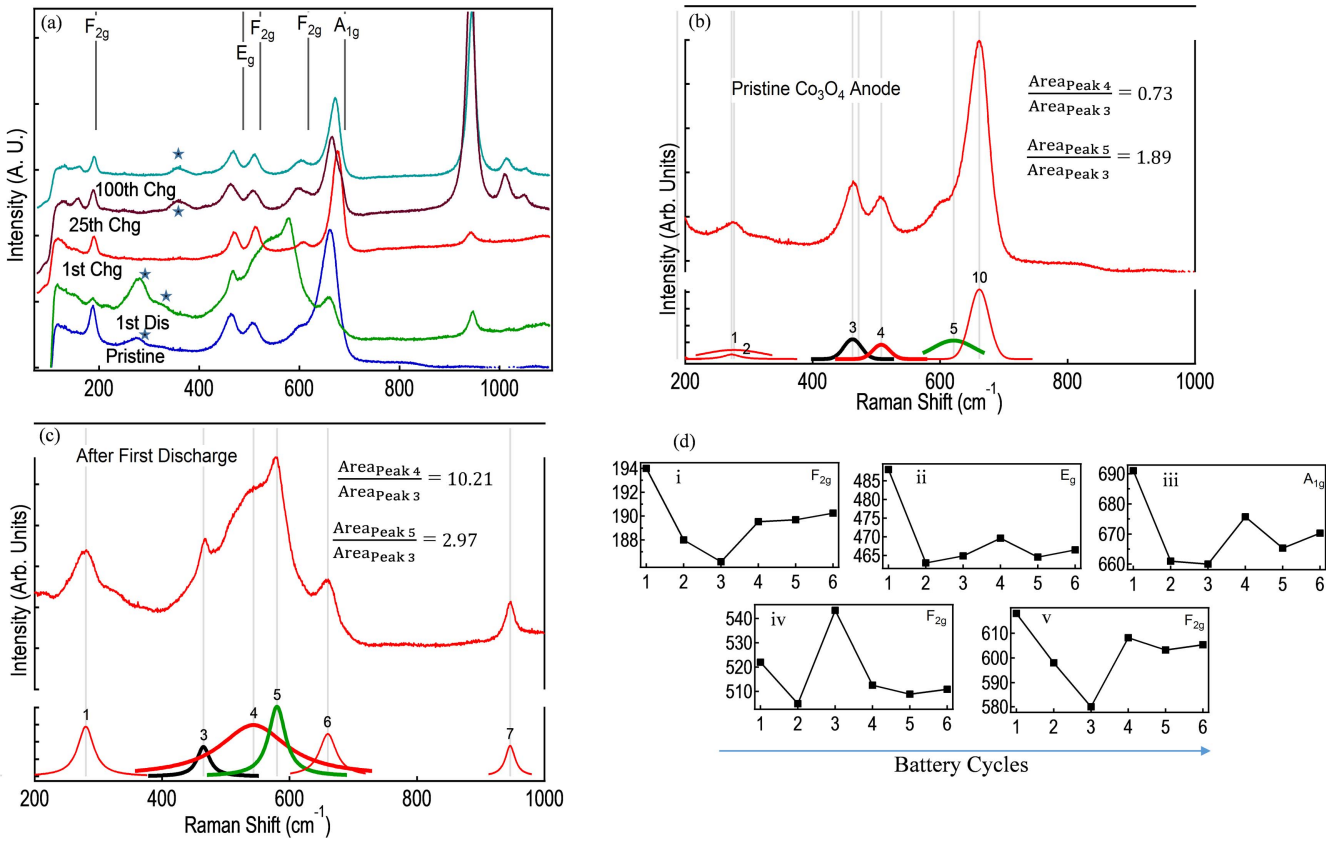

Figure 3. Raman spectra of Co_3O_4 nanoparticle anodes. In the Raman spectra (a) from the Co_3O_4 nanoparticle anodes at different stages of the battery cycling, the copper oxide peaks are shown with asterisks and the peak position of bulk Co_3O_4 are shown with vertical lines. Lorentzian fits to the Raman spectra from pristine Co_3O_4 nanoparticle anodes (b) and from the anode after the first discharge cycle (c) show the Raman signatures of Li_2O upon discharging of the battery. The trends in Raman peak positions show signatures of strain relaxation in Co_3O_4 nanoparticles. For clarity the trends of these peaks are shown individually in (d). The *x*-axes labels in (d) correspond to battery cycle index. 1—Co_3O_4 bulk, 2—Co_3O_4 nanoparticle pristine anode, 3—Co_3O_4 nanoparticle anode after first discharge, 4—Co_3O_4 nanoparticle anode after 1 discharge/charge, 5—after 25th charge, 6—after 100th charge.

Table 1. The Raman peak positions at different stages of battery cycles.

Battery activity ↓	F_{2g}	E_g	F_{2g}	F_{2g}	A_{1g}
Bulk Co_3O_4	194	488	522	618	691
Pristine electrode	188	463	505	598	661
Fist discharge	186.5	465	543.5	580.5	660.0
Fist discharge/charge	189.5	469.5	512.5	608.0	676
25th discharge/charge	190	465	509	603.0	665.5
100th discharge/charge	190.25	466.5	511	605.5	670.5

Nanoscale unique properties, e.g., quantum confinement, surface strain, impurities, etc, are extremely important for battery performance and these are the same properties that can be studied extensively with Raman spectroscopy. We performed Raman studies on the Co_3O_4 nanoparticle anodes at the following stages of the battery cycling: the pristine Co_3O_4 nanoparticle anodes, after the first discharge of the battery, after first discharge/first charge cycle, after 25 cycles of discharge/charge at various rates, and after 100 cycles of discharge/charge. Figure 3(a) and table 1 summarize the Raman spectra from each of these samples along with the bulk values acquired from literature [41]. In summary, our studies show clearly that Co_3O_4 nanoparticles convert to elemental Co and LiO_2 when the battery discharges. However, our results also indicate that the nanoparticles may not completely reconstitute back to their initial spherical shapes upon re-charging, a result that is of significance but has so far received scant attention.

Before discussing the Raman spectra from the EPD Co_3O_4 nanoparticle film anodes we note that since all the data were collected from the nanoparticle anodes with the copper substrates that were annealed in the oven for 6 h at 200 °C there must be contribution from copper oxide to the overall Raman spectra. The copper oxide peaks are shown in figure 3(a) with asterisks. The position, shift, and evolution of these peaks are similar to what Akgul *et al* observed in their Raman study of copper oxide thin films grown on glass substrates [42], and in our case can be explained by continuous oxidation and crystallization of the copper oxide substrate as a result of temperature rise inside the LIBs. Since this is not relevant to the physics of nanoparticle based LIBs, we will not discuss this effect in this paper.

Co_3O_4 crystallizes in the normal spinel structure $Co^{2+}(Co^{3+})_2(O^{2-})_4$ with the space group $Fd\bar{3}m$ (Number 227). Co^{2+} and Co^{3+} occupy the tetrahedral and octahedral sites, respectively. The primitive unit cell contains 14 atoms. Normal mode enumeration shows that the normal spinel crystal structure has 27 optical modes and are classified as $A_{1g}(R) + E_g(R) + 2A_{2u}(IR) + 2E_u(IR) + 3F_{2g}(R) + F_{1g}(R) + 2F_{2u}$. The $A_{1g}(R)$, $E_g(R)$ and the $F_{2g}(R)$ modes are Raman active [43]. Hadjiev *et al* and Alrehaily *et al* conducted Raman studies of bulk Co_3O_4 [41, 44]. The former group, conducting the spectroscopic study at 312 K, observed the following five peaks: F_{2g} at 194 cm^{-1}, E_g at 488 cm^{-1}, F_{2g} at 522 cm^{-1}, F_{2g} at 618 cm^{-1} and A_{1g} at 691 cm^{-1}. Our Raman spectrum, as shown in figure 3(a) and table 1, from pristine Co_3O_4 nanoparticle electrodes show the following results: F_{2g} at 188 cm^{-1}, E_g at 463 cm^{-1}, F_{2g} at 505 cm^{-1}, F_{2g} at 598 cm^{-1} and A_{1g} at 661 cm^{-1}. When compared to the bulk Raman signatures we observe an across the board red shift which is a unique signature of Raman spectra of nanoparticles.

The Raman spectra from nanoparticles can be drastically different from their bulk counterparts due to a myriad of factors including, but not limited to, phonon confinement, strain, size distribution, defects and variations in phonon relaxation with particle size. Phonon confinement is related to the fact that whereas in the bulk, only the zone center modes can be Raman active, in nanomaterials an increasing volume of the reciprocal lattice space is sampled in Raman scattering and modes other than those at the zone center can become Raman active. Strain in nanoparticles is a well-known phenomenon with increasing strain as the particle size decreases [20, 21]. Size distribution leads to dispersion in lattice constants and inhomogeneous strain which manifests as inhomogeneous broadening in the Raman spectra. In oxide materials the major source of defects is oxygen vacancies and the resulting valence change of metals which, in turn, results in strain in oxide nanoparticles.

In $CeO_{(2-y)}$ nanoparticles Spanier *et al* observed progressive red shift of the triply degenerate first order Raman line at 464 cm^{-1} that could be explained through increasing lattice constant with decreasing particle size and consequently, increasing strains, and phonon confinement [45]. Strain and phonon confinement, however, are not necessarily spatially homogeneous and as such their influence on normal modes of different symmetries could be different. For some cases the peak shift due to strain could be in opposite direction from that due to phonon confinement, and for those modes the overall shift could be smaller or even non-existent as nanoparticle size decreases [45].

As shown in figure 3(a) and table 1, the Raman spectrum collected from our pristine Co_3O_4 nanoparticle anode shows results that are very similar to what Spanier *et al* observed, namely a red shift of the prominent Raman peaks, ranging from a minimum of 6 cm^{-1} for the F_{2g} peak to a maximum of 30 cm^{-1} for the A_{1g} peak.

The discharge of LIBs produces elemental cobalt and Li_2O, as shown in equation (1). Raman spectrum from the first discharge cycle of our H-LIB is shown in figure 3(a) and more clearly in figure 3(c), and reveals several key factors relevant to the electrochemistry of the battery. First of all, three out of five of the Raman peaks of the original material Co_3O_4 nanoparticles are still present. These F_{2g} (186.17 cm^{-1}), E_g (464.85 cm^{-1}), and A_{1g} (660.06 cm^{-1}) peak positions are almost identical to those from the pristine electrode. This indicates the reaction is incomplete and all of the anode material is not converted into elemental Co and Li_2O. Two additional peaks, however, at 543.5 and 580.5 cm^{-1} seen in the spectra are significantly different from those of the original Co_3O_4 nanoparticles.

The Raman signature of the conversion of Co_3O_4 into Co and Li_2O is complicated by the fact that the Raman peaks of Li_2O are approximately at the same position as those of the two higher F_{2g} peaks of Co_3O_4. Sanchez-Carrera *et al* performed first principle calculations of the normal modes of lithium oxides—both Li_2O and Li_2O_2—and compared those with experimental Raman spectra [46]. The main Raman peak of Li_2O was found to be at 523 cm^{-1} experimentally and DFT calculations of a molecular crystal of with two units of Li_2O determined this mode frequency to be 566 cm^{-1}. We believe the peaks at 543.5 and 580.5 cm^{-1} seen in our spectrum are due to Li_2O and the homogeneous phase $Li_xCo_3O_4$ that are known to form due to Li^+ ion insertion into the electrode lattice [11]. Shift of Raman peaks due to changes in the reduced mass of Raman modes is a well understood phenomenon [47]. As for the missing Co_3O_4 nanoparticle peaks we believe these F_{2g} peaks are enveloped by the larger Li_2O peaks.

Further indications of the peaks at 543.5 and 580.5 cm^{-1} being contributed by Li_2O are the ratios of the areas of these peaks to the nearby E_g peak between the Raman spectra from pristine Co_3O_4 nanoparticles (figure 3(b)) and the spectra after the first discharge (figure 3(c)). As shown in the insets of figures 3(b) and (c), the ratios increase from less than one to more than ten for the first peak and from less than two to almost three for the latter peak.

The next Raman spectrum was from the H-LIB after the first discharge/charge cycle, as shown in figure 3(a). Peak fitting of the spectra show that all five Co_3O_4 nanoparticle Raman peaks appear at this condition. However the peaks have blue shifted compared to those from the pristine samples indicating that the Co_3O_4 matrix is now relaxed compared to the pristine nanoparticles. Subsequent Raman spectra taken after 25 cycles of discharge/charge and 100 cycles of discharge/charge show the presence of all five modes from Co_3O_4 and progressive but uneven blue shifts of the peaks indicating even more relaxation. For clarity the trends of these peaks are shown individually in figure 3(d), where it is seen clearly that—except for the disruption caused by the Li_2O peaks at first discharge, as shown in panel iv—the Co_3O_4 nanoparticle peaks start out red shifted compared to the bulk value but as the battery undergoes many cycles the peaks start to recover, blue shift and get closer to bulk Co_3O_4.

The appearance of all five Raman modes after 100 cycles of the H-LIB is a clear indication that the anode material is Co_3O_4 nanoparticles as opposed to CoO that previous reports

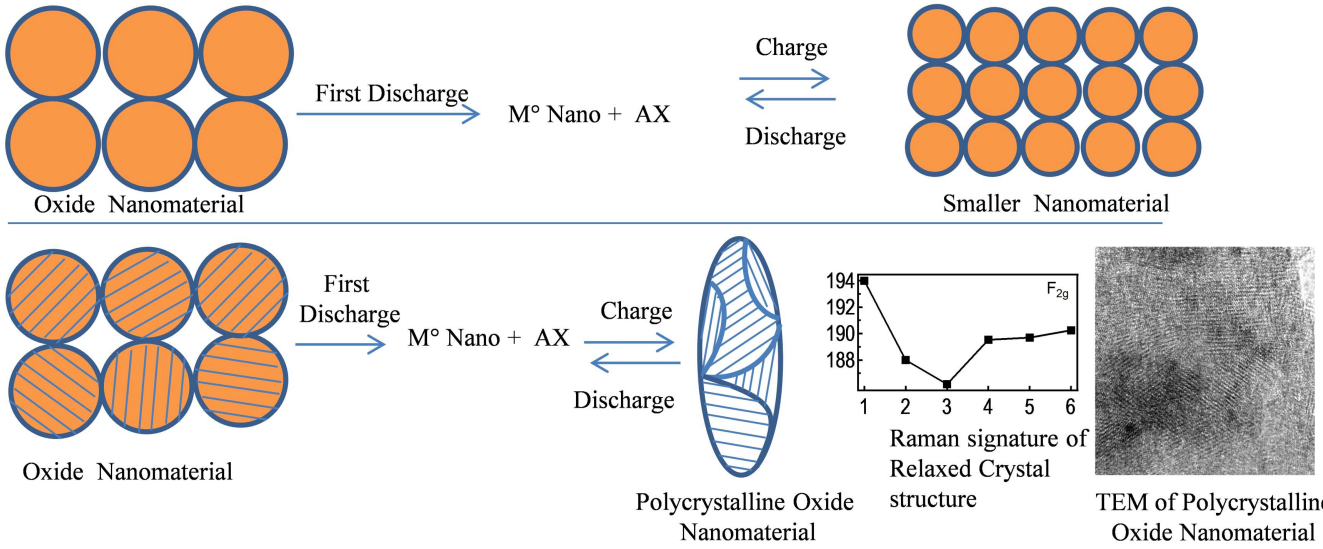

Figure 4. Top panel: conversion reactions in LIBs composed of nanostructured electrodes; as reported in some research articles the large size nanoparticles get pulverized into smaller one leading to stable charging/discharging [5]. Bottom panel: in our H-LIBs with Co_3O_4 nanoparticle film anodes we observed transformation of nanoparticles films into polycrystalline materials. Raman spectra collected from the H-LIBs show red shift of the Co_3O_4 F_{2g} mode between bulk (*x*-axis label 1) and pristine nanoparticles (*x* label 2), indicating increased lattice constant and tensile strain. As the battery undergoes cycles (*x* labels 3, 4, 5, 6) the F_{2g} mode blue shifts pointing toward lattice relaxation and polycrystallinity. TEM images (lower panel) collected from used Co_3O_4 nanoparticles scrapped off the electrodes after 100 H-LIB cycles support our assertion.

have claimed [7]. While it is true that the known Raman peaks of CoO at 471 and 668 cm^{-1} are close to those of Co_3O_4 as shown in table 1, we believe it is more probable—based on the appearance of all five Co_3O_4 Raman modes—that the anode material upon 100 cycles of discharge/charge is Co_3O_4.

The appearance of Raman peaks at energies of 944 cm^{-1} and beyond in all the electrodes except for the pristine electrode in our H-LIBs could result from species resulting from electrolyte-nanoparticle and electrolyte-copper oxide reactions.

High capacity and high speed rechargeable batteries operating in the conversion reaction mode require the anode and cathode materials to undergo complete chemical changes in each half cycle, often at different rates. This places significant demand on the electrochemistry of these batteries as seen from the rate dependence of the battery capacitance; as seen in figure 2(c), as the cycle rate is increased the battery capacitance decreases. Additionally, since the lattice constants of the reactants and products are different (equation (1)) the electrode materials undergo significant amount of expansion and contraction at each cycle which affects the mechanical stability of the electrodes and very often results in pulverization leading to degradation of the battery. While nanoparticles possess the unique characteristics of being able to accommodate strain through volume expansion without pulverization and consequently without significant capacity fading there have been little study of the actual physical mechanism of this effect. It is obvious that the mechanism of lithiation for electrodes composed of quasi-spherical nanoparticles will be different from those composed of planar thin films. Nanoparticles are already under tensile strain due to the increase of lattice constant with decreasing particle size and it is not obvious how the strain accompanied by lithiation and chemical conversion affect their overall crystal structure. Previous efforts to determine the electrochemistry in LIBs mostly focused on the gravimetric capacity. However, for light-weight batteries parasitic capacitance can play an outsize role, and as such it is difficult to determine how much of the anode materials participate in the charge/discharge processes.

The authors of [5] claimed that after the first cycle the larger size nanoparticles get pulverized into smaller ones (figure 4, top panel). However, we believe the TEM images that were used to make this claim do not clearly show individual smaller nanoparticles. Additionally, no justification was presented for why the nanoparticles will settle down on a specific size and not continue to get pulverized. We believe, on the contrary, that the large nanoparticles do not break down into smaller ones upon discharging and charging, based on the fact that in our experiments the Raman peaks after the first discharge/charge cycle do not show continuous red shift corresponding to higher strains from smaller nanoparticles. On the contrary, the peaks, as seen from figure 3(d), show signs of blue shift or strain release. TEM collected from used Co_3O_4 nanoparticles scrapped off the electrodes after 100 H-LIB cycles (figure 4 bottom panel) clearly shows polycrystalline domains. The same TEM is shown with better clarity in figure S5 in the supplementary information. We believe this shows that in the equilibrium, after several cycles the anode material acquires a polycrystalline structure which is able to accommodate the strain imposed by lithiation more efficiently compared to the bulk materials or nanoparticles. We show such effects schematically in figure 4, bottom panel.

Conclusion

Fundamental electrochemistry of Co_3O_4 nanoparticle anode based H-LIBs is investigated through TEM, SEM, AFM, galvanostatic charge/discharge cycles, CV, and Raman spectroscopy. The batteries were found to possess long cycle lives with two hundred charge/discharge cycles with at least 50% retention of the initial capacity. Raman spectroscopy reveals that an incomplete conversion of the Co_3O_4 nanoparticle into Li_2O and elemental Co takes place after a full discharge process and that as the charge/discharge processes continue the nanoparticles experience strain relaxation. This strain relaxation point to Li_2O and elemental Co not fully reconstituting into the original Co_3O_4 nanoparticles upon a charge cycle.

Acknowledgments

This work made use of the Cornell Center for Materials Research Shared Facilities, which are supported through the NSF MRSEC program (DMR-1719875).

MI, MZ, VD and NN gratefully acknowledge the SUNY Oswego SCAC grant for the year 2015–2016 for support of this work.

CJW gratefully acknowledges the US Army Research Office under a DURIP award and the Centralized Research Facilities at Drexel University.

ORCID iDs

Mohammad A Islam https://orcid.org/0000-0002-8617-4858

References

[1] Bagotsy V S 2006 *Fundamentals of Electrochemistry* (Hoboken, NJ: Wiley)
[2] Cabana J, Monconduit L, Larcher D and Palacin M 2010 *Adv. Mater.* **22** E170
[3] Stephenson T, Li Z and Olsen B 2014 *Energy Environ. Sci.* **7** 209
[4] Chang K and Chen W 2011 *ACS Nano* **5** 4720
[5] Ha D-H, Islam M and Robinson R 2012 *Nano Lett.* **12** 5122
[6] Kim Y *et al* 2014 *ACS Nano* **8** 6701
[7] Poizot P, Laruelle S, Grugeon S, Dupont L and Tarascon J 2000 *Nature* **407** 496
[8] Liu H-C and Yen S K 2007 *J. Power Sources* **166** 478
[9] Chan C, Peng H, Liu G, McIlwrath K, Zhang X, Huggins R and Cui Y 2008 *Nat. Nano* **3** 31
[10] Taberna P, Mitra S, Poizot P, Simon P and Tarascon J 2006 *Nat. Mater.* **5** 567
[11] Wang H, Yang Y, Liang Y, Robinson J, Li Y, Jackson A, Cui Y and Dai H 2011 *Nano Lett.* **11** 2644
[12] Liu B, Xu X, Luo W, Sun Y and Huang Y 2014 *Sci. Rep.* **4** 04229
[13] Kim S, Naguib M, Zhao M, Zhang C, Jung H-T, Barsoum M and Gogotsi Y 2015 *Electrochem. Acta* **163** 246
[14] Das S, Mallavajula R, Jayaprakash N and Archer L 2012 *J. Mater. Chem.* **22** 12988
[15] Chockla A, Harris J, Akhavan V, Bogart T, Holmberg V, Steinhagen C, Mullins C, Stevenson K and Korgel B 2011 *J. Am. Chem. Soc.* **133** 20914
[16] Singh V, Kosa M, Majhi K and Major D T 2015 *J. Chem. Theory Comput.* **11** 64
[17] Wang D, Yu Y, He H, Wang J, Zhou W and Abruña H 2015 *ACS Nano* **9** 1775
[18] Gu D, Li W, Wang F, Bongard H, Spliethoff B, Schmidt W, Weidenthaler C, Xia Y, Zhao D and Schüt F 2015 *Angew. Chem., Int. Ed. Engl.* **54** 7060
[19] Li B, Cao H, Shao J, Li G, Qu M and Yin G C 2011 *Inorg. Chem.* **50** 1628
[20] Tsunekawa S, Sahara R, Kawazoe Y and Ishikawa K 1999 *Appl. Surf. Sci.* **152** 53
[21] Tsunekawa S, Ishikawa K, Li Z-Q, Kawazoe Y and Kauya Y 2000 *Phys. Rev. Lett.* **85** 3440
[22] Puntes V, Krishnan K and Alivisatos P 2011 *Science* **291** 2115
[23] Yin Y, Rioux R, Erdonmez C, Hughes S, Somorjai G and Alivisatos A 2004 *Science* **304** 711
[24] Ha D-H, Ly T, Caron J, Zhang H, Fritz K and Robinson R 2015 *ACS Appl. Mater. Interface* **7** 25053
[25] Chen J, Ye X, Oh S, Kikkawa J, Kagan C and Murray C 2013 *ACS Nano* **7** 1478
[26] Islam M and Herman I 2003 *Appl. Phys. Lett.* **80** 3823
[27] Islam M, Xia Y, Yin M, Liu Z, O'Brien S, Levicky R and Herman I 2003 *Nano Lett.* **3** 1603
[28] Islam M, Xia M, Telesca D, Steigerwald M and Herman I 2004 *Chem. Mater.* **16** 49
[29] Otelaja O, Ha D-H, Ly T, Zhang H and Robinson R 2014 *Appl. Mater. Interfaces* **6** 18911
[30] Chen Q, Li W, Goudouri O M, Ding Y, Cabanas-Polo S and Boccaccini A R 2015 *Colloids Surf.* B **130** 199
[31] Chavez-Valdez A, Shaffer M, Xia M and Boccaccini A 2013 *J. Phys. Chem.* **117** 1502
[32] Choi H, Hwang S, Bae H, Kim S, Kim H and Jeon M 2011 *Electron. Lett.* **47** 281
[33] Xu G-L, Li J-T, Huang L, Lin W and Sun S-G 2013 *Nano Energy* **2** 394
[34] Spanier J, Levy M, Herman I, Osgood R and Bhalla A 2001 *Appl. Phys. Lett.* **79** 1510
[35] Yuzyuk Y, Alyoshin V, Zakharchenko I, Sviridov E, Almeida A and Chaves M 2002 *Phys. Rev.* B **65** 134107
[36] Dore P, Postorino P, Sacchetti A, Baldini M and Giambel-luca R 2005 *Eur. Phys. J.* B **48** 255
[37] Kreisel J, Weber M, Dix N, Sánchez F, Thomas P and Fontcuberta J 2012 *Adv. Funct. Mater.* **22** 5044
[38] Iliev M, Guo H and Gupta A 2007 *Appl. Phys. Lett.* **90** 15191
[39] Aroca R, Nazri M, Nazri G, Camargo A and Trsic M 2000 *J. Solut. Chem.* **7** A82
[40] Battisti D, Nazri G, Klassen B and Aroca R 1993 *J. Phys. Chem.* **97** 5826
[41] Hadjiev H, Iliev M and Vergilov I 1988 *J. Phys. C: Solid State Phys.* **21** L199
[42] Akgul F A, Akgul G, Yildirim N, Unalan H E and Turan R 2014 *Mater. Chem. Phys.* **147** 987
[43] Kroumova E, Aroyo M, Perez Mato J, Kirov A, Capillas C, Ivantchev S and Wondratschek H 2003 *Phase Transit.* **76** 155
[44] Alrehaily L, Joseph J, Biesinger M, Guzonas D and Wren J C 2013 *Phys. Chem. Chem. Phys.* **15** 1014
[45] Spanier J, Robinson R, Zhang F, Chan S and Herman I P 2001 *Phys. Rev.* B **64** 245407
[46] Sanchez-Carrera R and Koznsky B 2014 *Phys. Chem. Chem. Phys.* **16** 24549
[47] Islam M, Rondenelli J and Spanier J 2016 *J. Phys.: Condens. Matter* **27** 155401